Effect of Valence and Chemical Species of Added Electrolyte on Polyelectrolyte Conformations and Interactions

Gina A. Sorci† and Wayne F. Reed*

Physics Department, Tulane University, New Orleans, Louisiana 70118

Received October 15, 2003; Revised Manuscript Received November 11, 2003

ABSTRACT: The effect of added electrolyte (AE) valence and species on polyelectrolytes was studied using automatic, continuous mixing (ACM), allowing measurements over composition gradients. The second virial coefficient A_2 was decomposed into contributions from an electrostatically sensitive mean-square gyration radius $\langle S^2 \rangle$ and an external electrostatic field. $\langle S^2 \rangle$ matched predictions of combined electrostatic persistence length and excluded-volume theories, without adjustable parameters. A_2 was modeled via an equivalent, soft-core, expansible, charged sphere. Whereas the scaling behavior of $\langle S^2 \rangle$, intrinsic viscosity $[\eta]$, and A_2 was the same for all AE, the prefactors strongly depended on AE symmetry and valence. At given ionic strength $\langle S^2 \rangle$, $[\eta]$, A_2, effective linear charge density, and expansible sphere surface potential are less for divalent than monovalent AE. Different ion species for a given valence class showed second-order effects following a Hoffmeister series. ACM should also prove valuable for investigating AE-induced phase transitions in polyelectrolytes like DNA and proteins.

Introduction

The effects of ionic strength on polyelectrolyte conformations have been studied experimentally and theoretically for many years.[1] The main qualitative trends for semiflexible, linear polyelectrolytes have been confirmed amply for many different types of polyelectrolytes with a variety of techniques. In short, it is expected on basic principles, and generally found experimentally, that as ionic strength increases the ionic shielding leads to a steady contraction of the individual chain static and hydrodynamic dimensions, e.g., a reduction in mean-square radius of gyration $\langle S^2 \rangle$ and intrinsic viscosity $[\eta]$, respectively. Likewise, the interparticle interactions decrease with increasing ionic strength, e.g., as manifested by decreasing second, third, and higher virial coefficients (A_2, A_3, etc.). For some polyelectrolytes, these properties change smoothly, whereas others exhibit phase transitions, such as those seen for DNA and many proteins in the presence of higher valence salts and different ion species.

Ion specificity is frequently encountered in charged macromolecular and colloidal structures. In Ninham and Yaminsky's[2] study of SDS and CTAB, the ion specific effects are described by including the dispersion interactions acting on ions together with electrostatics instead of treating them separately. In particular, ion specificity is commonly found in many biological systems,[3−5] where ions such as Ca^{2+} play a special role, apart from their mere valence. An example is the ability of multivalent ions to "condense" DNA. Different valences have also been found to induce different helical structures and in some cases cause a coil−helix transition.[6,7]

Most polyelectrolyte theories assume that the ions responsible for creating the ionic atmosphere around the macroions can be treated as point charges. If this assumption is true, then a whole layer of potential difficulties involving ion species, and discrete vs continuum effects can be avoided. Early reports of ionic specificity in polyelectrolytes by Flory and Osterheld[8] can be traced back to the 1950s, and much earlier for colloids, where it had been recognized that valence far outweighed chemical species in terms of stability and gelation.[9,10] The Flory and Osterheld experiments involved the intrinsic viscosity of poly(acrylic acid) in the presence of different salts NaCl, $CaSO_4$, and $CaCl_2$ and demonstrated that changing the anion in monovalent salts had little effect but that when the valence was changed from monovalent to divalent the effects were much larger, suggesting a purely electrostatic effect. In later works by Orofino and Flory[11] and by Overbeek and Vrij,[12] light scattering was used to study the effects of monovalent salts on polyelectrolytes. Orofino and Flory were concerned with A_2 effects caused by the different monovalent salts, while Overbeek et al. measured what they call the apparent molecular weight and A_2 and analyzed them in terms of specific ion adsorption/desorption on the polyion. Flory and Orofino calculated these latter effects to be negligible. They described the differences between the ion species of the same valence in terms of the activity of the ions near the polyelctrolyte. In more recent work by Beer et al.,[13] similar effects to those in this work were observed, which show that in the presence of a polyanion the size of the anion has a larger effect than the co-ion. They modeled these effects using fits of experimental data and excluded-volume theory. Other even more dramatic ion specific effects occur when DNA is exposed to multivalent ions.[14,15] Hydration forces between condensed DNA rods have been observed by X-ray techniques.[16,17] In another example, DNA is condensed into a torus shape when exposed to such ions as spermine, $Co(NH_3)_6$, or even divalent ions in mixed alcohol/aqueous solution.[18] The mechanisms of condensation are believed to be manifold, including electrostatic, hydration, and entropically based forces. In another study of DNA the Mn^{2+} causes the DNA to aggregate by linking the ends of DNA chains together creating long strands.[19]

The purpose of this work is twofold: to present the potential of the automatic continuous mixing technique for studying the detailed behavior of polyelectrolytes and

† Current address: Department of Physics, Millsaps College, Jackson, MS 39210.

* Corresponding author.

10.1021/ma035551z CCC: $27.50
Published on Web 12/23/2003

to take advantage of the continuous record of polymer behavior as the component mixture changes via ACM, to investigate the role that different types of electrolytes have on polyelectrolyte conformations and interactions. Sodium hyaluronate (HA) has been chosen for this work as an example of a well-behaved linear polyelectrolyte. It does not undergo conformational collapse like DNA but rather passes continuously and smoothly between states produced by the different ion concentrations and types. Furthermore, the type of HA used here is free of any aggregates, such as have clouded many past polyelectrolyte studies. ACM allows even small changes in scattering and viscosity behavior to be monitored. With these data it is then possible to ferret out which effects are sterically based and which might be based purely on the interaction of electrostatic fields and differentiate the effects of added electrolyte valence and chemical species. The electrolytes studied here include different species of symmetric mono- and divalent and asymmetric divalent electrolytes.

Background Notions

Theories for polyelectrolytes often begin with the Poisson−Boltzmann (PB) equation. Many of these theories use the linearized form of the PB in order to arrive at analytical results that furnish insight into the overall trends in polyelectrolyte behavior.

A key notion resulting from the PB equation is that of the electrostatic (or Debye) screening length, which is given, for symmetric electrolytes by

$$\kappa^{-1} = \left(\frac{\epsilon kT}{2Ie}\right)^{1/2} \tag{1}$$

where I is the ionic strength, defined by

$$I = \frac{1}{2}\sum_{i=1}^{n} [\mathrm{A}_i] z_i^{\,2} \tag{2}$$

where $[\mathrm{A}_i]$ is the molar concentration of ion type i in an added electrolyte of bulk concentration [E], z_i is the charge on ion type A_i, and n is the total number of ion species. Although semiflexible polyelectrolytes are ill-suited to be modeled as spheres, there is often an "equivalent sphere" notion for most properties (e.g., hydrodynamic radius). Therefore, it is useful to recall the form of the electrostatic potential in the spherically symmetric case

$$\phi(r) = \frac{\sigma R_{\mathrm{eq}}^{\,2} \mathrm{e}^{\kappa R}}{\epsilon(1 + \kappa R_{\mathrm{eq}})} \frac{\mathrm{e}^{-\kappa r}}{r} \tag{3}$$

where R_{eq} is the "equivalent electrostatic sphere's" radius and σ its surface charge density. When there is no shielding $\kappa = 0$, and eq 3 then recovers its unscreened form $\sigma R^2/\epsilon r$. The interaction between the equivalent spheres in dilute solution can be measured via the second virial coefficient A_2, which is composed of the hard-sphere potential (first term in the following equation) and any "soft" potential, such as an electrostatic field, represented by the integral term in the following expression

$$A_2 = \frac{N_{\mathrm{A}}}{2M^2}\left[\frac{32\pi R_{\mathrm{eq}}^{\,3}}{3} + 4\pi\int_{2R_{\mathrm{eq}}}^{\infty} [1 - \exp(-U(r_{12})/k_{\mathrm{B}}T]] r_{12}^{\,2}\, \mathrm{d}r_{12}\right] \tag{4}$$

where $U(r_{12})$ is the interaction potential energy of the spheres whose centers are separated by a distance r_{12}.

The polyelectrolyte properties directly measured in this work are $\langle S^2\rangle$, A_2,[20] and $[\eta]$. There are abundant polyelectrolyte theories for $\langle S^2\rangle$, A_2, and $[\eta]$. The unperturbed value of $\langle S^2\rangle$ is that found in a Θ-solvent (i.e., where there are no excluded-volume interactions), and this is often denoted $\langle S^2\rangle_0$. In the so-called wormlike chain model $\langle S^2\rangle_0$ is given in terms of the total contour length of the polymer L and the total persistence length L_{p}. The wormlike chain expression for a random coil with no excluded volume is[21]

$$\langle S^2\rangle_0 = \frac{LL_{\mathrm{p}}}{3} - L_{\mathrm{p}}^{\,2} + 2L_{\mathrm{p}}^{\,3}/L - 2\left(\frac{L_{\mathrm{p}}^{\,4}}{L^2}\right)[1 - \exp(-L/L_{\mathrm{p}})] \tag{5}$$

where L is the contour length of the polymer and L_{p} the persistence length. The measured $\langle S^2\rangle$ for a polyelectrolyte is larger than $\langle S^2\rangle_0$ due to electrostatic excluded-volume effects, but these effects cannot be distinguished from local stiffening effects experimentally. Hence, in earlier works $\langle S^2\rangle_0$ was replaced by $\langle S^2\rangle$, and the resulting persistence length obtained from eq 5 was termed the "apparent persistence length", L_{p}'. $\langle S^2\rangle$ is computed by a procedure previously summarized.[22] Namely, following Odijk[23,24] and Skolnick and Fixman,[25,26] it is assumed that at any value of ionic strength the total persistence length is the sum of the intrinsic persistence length $L_{\mathrm{p},0}$ and an electrostatic persistence length (EPL), or L_{e}, where L_{e} is normally a small perturbation to $L_{\mathrm{p},0}$. That is $L_{\mathrm{p}} = L_{\mathrm{p},0} + L_{\mathrm{e}}$, and L_{e} was computed to be

$$L_{\mathrm{e}} = \frac{\xi^2\kappa^{-2}}{12\lambda_{\mathrm{B}}}\left[3 - \frac{8}{y} + \mathrm{e}^{-y}\left(y + 5 + \frac{8}{y}\right)\right] \tag{6}$$

where ξ is the number of elementary charges per Bjerrum length (7.18 Å in water at 25 °C) and $y = \kappa L$. With knowledge of $L_{\mathrm{p},0}$ obtained at very high ionic strength, L_{p} can hence be computed from eq 6, so that $\langle S^2\rangle_0$ can be computed by eq 5. The measured value $\langle S^2\rangle$ is related to $\langle S^2\rangle_0$ via the static expansion factor α_{s}

$$\langle S^2\rangle = \alpha_{\mathrm{s}}^{\,2}\langle S^2\rangle_0 \tag{7}$$

There are several theories that relate α_{s} to the usual perturbation parameter z, given by

$$z = \left(\frac{3}{2\pi L_{\mathrm{k}}^{\,2}}\right)^{3/2} \beta N_{\mathrm{k}}^{\,1/2} \tag{8}$$

where L_{k} and N_{k} are the (Kuhn) statistical segment length and number, respectively, and $L_{\mathrm{k}} = 2L_{\mathrm{p}}$ in the unperturbed coil limit. Here β is the excluded volume between two charged rodlike segments, for which Fixman and Skolnick arrived at the expression

$$\beta = 8L_{\mathrm{p}}^{\,2}\kappa^{-1}\int_0^{\pi/2} \sin^{\,2}\theta \int_0^{w/\sin\theta} x^{-1}(1 - \mathrm{e}^{-x})\, \mathrm{d}x\, \mathrm{d}\theta \tag{9}$$

where

$$w = 2\pi\xi^2\kappa^{-1}e^{-\kappa d} \tag{10}$$

where d is the rod diameter.

Of the several expressions relating z to α_s, one that has found considerable utility when $N_k > 2$ is the Gupta−Forsman expression[27]

$$\alpha_s^5 - \alpha_s^3 \approx \frac{134}{105}(1 - 0.885N_k^{-0.462})z \tag{11}$$

It has frequently been found that the electrostatic excluded volume (EEV) contributes more to α_s than the EPL.[28,29]

The case of $[\eta]$ for linear polyelectrolytes is more complex, and although extensive theories exist,[30,31] there is not a fully developed consensus on which approximations work best. Typically, a viscometric expansion factor is introduced α_η, which relates $[\eta]$ to $[\eta]_0$, the intrinsic viscosity in Θ-solvent conditions. "Least draining" as opposed to "nondraining" can also have effects.[32]

It is noted that alternative approaches to computation of electrostatic effects on polyelectrolyte dimensions, such as those of Muthukumar,[33,34] have also proven successful.

Materials and Methods

Light Scattering Analysis. Analysis of the light scattered by homopolymers in dilute solution has traditionally been made via the Zimm equation

$$\frac{Kc}{R(q,c)} = \frac{1}{MP(q)} + 2A_2c + [3A_3Q(q) - 4A_2^2MP(q)(1 - P(q))]c^2 + O(c^3) \tag{12}$$

where $R(q,c)$ is the excess Rayleigh scattering ratio (cm^{-1}), that is, the total scattering of the solution at polymer concentration c minus that from the pure solvent. $P(q)$ is the form factor, and $Q(q)$ involves a set of Fourier transforms of the pairwise interactions. The scattering vector q is defined as $q = (4\pi n/\lambda)\sin(\theta/2)$.

Here K is an optical constant, given for vertically polarized light as

$$K = \frac{4\pi^2n^2(\partial n/\partial c)^2}{N_A\lambda^4} \tag{13}$$

In the limit as q goes to zero $Q(q)$ and $P(q)$ are equal to 1. The resulting equation is

$$\frac{Kc}{R(0,c)} = \frac{1}{M_w} + 2A_2c + 3A_3c^2 + O(c^3) \tag{14}$$

Alternate expressions for the semidilute regime based on scaling notions have also been reported.[35]

Referring to eq 12, in the case where $q^2\langle S^2\rangle < 1$, a useful approximation is

$$\frac{Kc}{R(q,c)} = \frac{1}{M_w}\left(1 + \frac{q^2\langle S^2\rangle_z}{3}\right) + 2A_2c \tag{15}$$

For ideal random coils in the limit where $q^2\langle S^2\rangle > 1$ a useful limiting expression is

$$\frac{Kc}{R(q,c)} = \frac{1}{2M_n} + \frac{\gamma q^2}{2} + 2A_2c \tag{16}$$

where M_n is the polymer number-average mass and

$$\langle S^2\rangle = \gamma M \tag{17}$$

and γ is independent of polydispersity and provides the scaling prefactor, assuming an ideal coil. Since HA has significant excluded-volume effects, the scaling law is closer to $M^{1.2}$. On the other hand, $q^2\langle S^2\rangle$ for HA in this work ranges from 1.5 to 6, exceeding the limit of eq 15. The $Kc/R(q,c)$ vs q^2 behavior, however, is quite linear, as shown below, suggesting that it might remain so to even lower q^2. Hence, eq 15 will be used throughout to provide a self-consistent basis for comparison of the ion type effects. It is noted that earlier work[36] used the high q equation to exploit the polydispersity independence. Persistence lengths resulting from that treatment are considerably shorter, by about a factor of $^2/_3$, than those found in this work using the low-q approximation. The model presented below, based on $\langle S^2\rangle$ from eq 15, will not change if eq 16 is used, but the values for L_p and related quantities will be lower. Polydispersity effects are ignored in this work.

In the case of polyelectrolytes there has historically been concern over the value of $\partial n/\partial c$ to be used in eq 12. It was shown that the proper refractive index increment to use is the one measured in dialysis equilibrium, with the polyelectrolyte and salt on one side of a membrane permeable only to the simple electrolyte and only the simple electrolyte on the other side.[12] This then gives the refractive index of the particle composed of the polyelectrolyte and its counterion cloud when the simple electrolyte is at constant chemical potential in the cloud and in bulk solution, $(\partial n/\partial c_1)_{\mu_s}$.

In principle, Vrij and Overbeek[12] provide a means of determining the selective adsorption factor of salt ions on the polyelectrolyte. Analyses are based on the fact that $(\partial n/\partial c_1)_{\mu_s}$ can be measured accurately. It has been shown in a review of such measurements that they vary enormously, by well over 30%, probably due in large part to the dialysis methodology and means of determining solute concentration.[37] Measurements during this work of the dialyzed value for HA varied by 18% between different determinations. On the other hand, there is no measurable difference in $\partial n/\partial c$, measured directly (without interposing the dialysis procedure) over a wide range of salt concentrations and valence and symmetry types and chemical species. For consistency, the highly reproducible nondialyzed value of 0.155 is used throughout.

Others working in this area have found the effect to be minimal, and it is often neglected.[8,9,38,39] It is pointed out that, at any rate, neither $[\eta]$ nor $\langle S^2\rangle$, as determined by the above method, is dependent on the value of $\partial n/\partial c$.

Viscosity Determinations. A single capillary viscometer was used where the capillary radius and the length were fixed. No calibration factor is needed since the voltage output is proportional to the pressure drop across the capillary and the proportionality factor cancels in the numerator and denominator of the reduced viscosity computation

$$\eta_r(t) = \frac{V(t) - V(0)}{V(0)\,c(t)} \tag{18}$$

The average shear rate in the capillary was around 500 s^{-1}. Most measurements were made at low enough concentrations that shear thinning effects could be ignored. The reduced viscosity is related to the intrinsic viscosity by

$$\eta_r = [\eta] + \kappa_H[\eta]^2c + \kappa_{H,2}c^2 + O(c^3) \tag{19}$$

Since the polymer concentration is usually small, the terms in c^2 and higher are neglected. Using individual ramps of polymer concentration in different ionic strengths of NaCl, $MgSO_4$, and $CaCl_2$ allowed extrapolation of the reduced viscosity to zero concentration to obtain the intrinsic viscosity. From these fits it was also possible to determine κ_H and hence use $\eta_r = [\eta] + \kappa_H[\eta]^2c$ to obtain $[\eta]$ for experiments done at finite c. For the different salts the κ_H values range from 0.05 to 0.4 and increase with I for each salt. ACM provides a means for concise and detailed determination of κ_H and its interpretation. This is left to future work.

The ACM Technique. The automatic, continuous mixing (ACM) technique allows a continuous gradient of solution

Table 1. Various Electrolytes Used and Their Values of $\partial n/\partial c$

salt	$\partial n/\partial c$	salt	$\partial n/\partial c$	salt	$\partial n/\partial c$
NaCl	0.174	$CaCl_2$	0.2273	CsCl	0.160
KBr	0.119	$MgCl_2$	0.252	NaF	0.131
NaBr	0.118	$MgSO_4$	0.168	KCl	0.132
NaI	0.141	NaAce	0.1366		

components to be formed along a desired path in composition space, using two or more solution reservoirs. The properties of the continuously varying solutions can be measured by an appropriate train of detectors. It is required that the mixed sample be in equilibrium or quasi-equilibrium. This latter restriction means that properties of the mixed solution at any instant do not change during the interval from mixing to measurement, typically about 100 s.

ACM has recently been used for determining properties of uncharged polymers,[40] effects of ionic strength on polyelectrolyte scattering and viscosity,[41,42] and complex association and polyelectrolyte behavior of charged surfactants and neutral polymers.[43]

The ACM technique was implemented using an ISCO 2060 pump with a 2050 gradient mixer attached. Following the pump was a 1 in. stainless steel frit filter holder in which was placed a 0.45 μm paper filter. The sample then passed through a Wyatt Technology (Santa Barbara, CA) Dawn DSP 18 angle light scattering detector followed by a single capillary viscometer and a Waters 410 refractometer. The Dawn DSP uses a vertically polarized helium−neon laser operating at 633 nm, and the flow cell used provides a range of usable angles in the range of 27°−145°. The data were collected and analyzed using software written in house.

Materials. The hyaluronic acid sodium salt from streptococcus zooepidemicus was purchased from Sigma. Separate gel permeation chromatography determinations gave $M_w = 1.8 \times 10^6$ g/mol and polydispersity indices of $M_z/M_w = 1.5$ and $M_w = 3$.[42] This value of M_w is in excellent agreement of that yielded by ACM. The solutions of pure HA were prepared in clean glassware using deionized, filtered water. A large amount of HA solution was prepared for consistency. The same stock solution was used for several experiments and was stored at 4°C for no longer than 3 days while the series of experiments were run. In previous work the consistency of the HA provided by Sigma was discussed, which included the reproducibility of light scattering experiments from different batches of HA.[42] The salts used were either purchased from Sigma or Aldrich and are listed in Table 1 along with their values of $\partial n/\partial c$. Values of the varying solute concentration, whether salt or polymer, were measured during ACM experiments using the refractometer.

Results and Discussion

First-Order Effects: Electrolyte Valence and Symmetry. It was found that the single largest effect on raw light scattering and viscosity data came from the valence and symmetry of the added electrolyte, similar to what has often been found for colloid stability.[9,10] Much smaller, but measurable, second-order effects were found among the valence classes when the chemical species of the ions was changed. This is treated below.

Figure 1a shows raw LS, viscometer, and RI data for an experiment in which the concentration of $CaCl_2$ was ramped from 0 to 1000 mM in three stages, 0−10, 10−100, and 100−1000 mM, while the concentration of HA remained constant at 0.1 mg/mL. The baseline of each instrument with pure H_2O is acquired over the first 1000 s, at which point the 0.1 mg/mL HA solution in pure water entered the detector stream. The high viscosity and very low scattering, scarcely above the water level, are hallmarks of the strong polyelectrolyte effects when unshielded in pure water. The dramatic

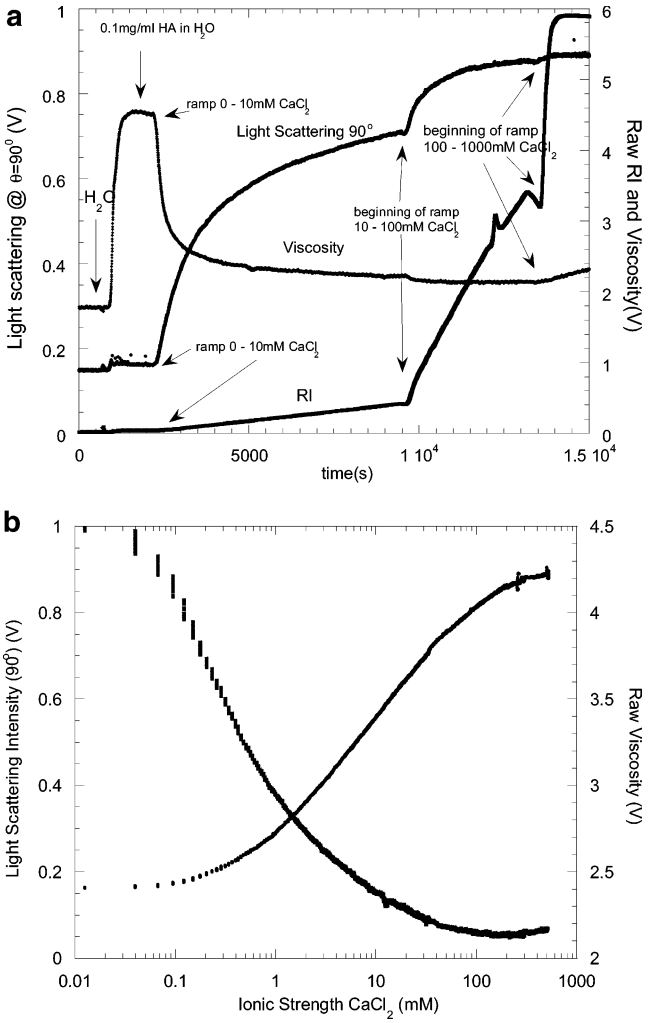

Figure 1. (a) Raw LS at 90°, viscometer, and RI data for a ramp of constant 0.1 mg/mL HA from pure water up to 1 M $CaCl_2$. Solvent conditions and procedure over each regime are indicated. (b) The raw LS at 90° intensity and viscosity vs $[CaCl_2]$, where $[CaCl_2]$ is determined from the RI data of (a).

increase in scattering as $CaCl_2$ is ramped up to 10 mM shows the profound effect that electrostatic screening has in reducing the electrostatically enhanced virial coefficients A_2, A_3, etc., in pure water. The 10−100 mM ramp in $CaCl_2$ produces noticeable but significantly less increase in scattering, indicating that shielding is largely complete by 10 mM, and the final ramp from 100 to 1000 mM produces almost no change in scattering. Meanwhile, it is significant that the viscosity "salts out" even more quickly than the light scattering and that early in the 0−10 mM ramp the viscosity essentially reaches its minimum. The slight increase in viscosity in going from 100 to 1000 mM is due to the contribution of the $CaCl_2$ itself to the solution viscosity. In subsequent analysis the regime from 1 to 1000 mM will be concentrated on to avoid the problem of how much ionic strength is added to the solution by the polyelectrolyte counterions themselves. This "self-salt" effect is prominent, for example, in the so-called electroviscous effect for polyelectrolytes.[44−48]

The RI signal in Figure 1a allows conversion of the data from the time domain into $[CaCl_2]$ and hence into ionic strength. Figure 1b shows raw light scattering and viscosity data vs I, where $[CaCl_2]$ was determined at each point by the RI. The procedural and temporal bias of the raw data in Figure 1a is completely removed in

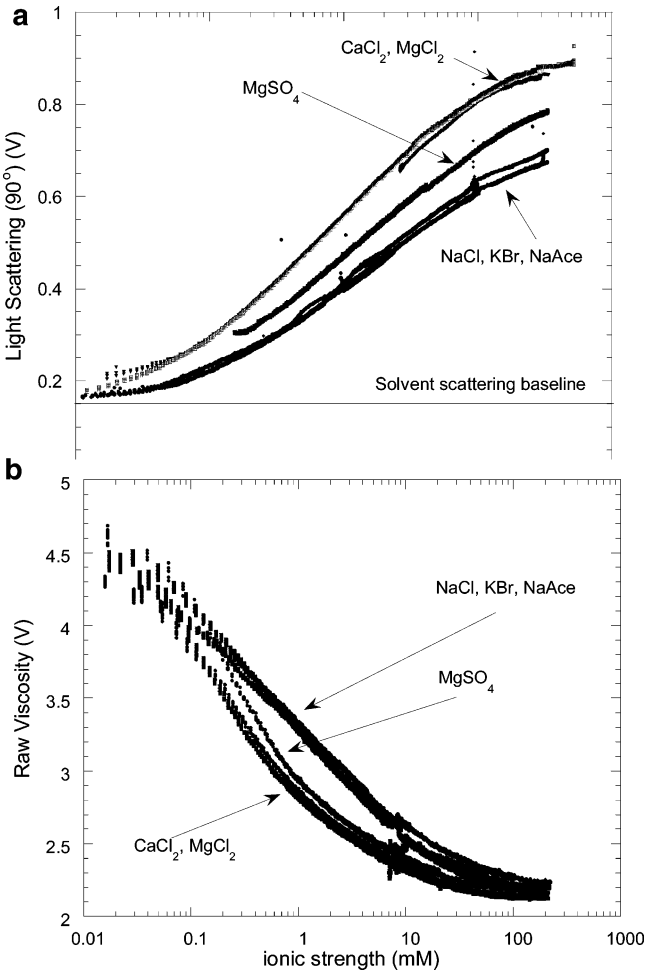

Figure 2. (a) Raw LS at 90° vs I (ionic strength) when 0.1 mg/mL HA is ramped from pure water to high I for each of several salts. (b) The raw viscosity data collected simultaneously with the data in (a).

this representation, and the monotonic effect that increasing [$CaCl_2$] has on both increasing scattering and decreasing viscosity is clearly seen.

Figure 2a shows typical raw light scattering behavior for 0.1 mg/mL HA vs ionic strength (I from eq 2) for different salts: the monovalents NaCl, KBr, and Na acetate, the single symmetric divalent $MgSO_4$, and the asymmetric divalents $CaCl_2$ and $MgCl_2$. As expected, the major effect of increased light scattering with increasing ionic strength is apparent for all salts. The magnitude of the effect, however, breaks into three distinct bands: the monovalent salts, which show the least variation, the asymmetric divalents, which show the greatest change, while the single symmetric divalent salt used shows an intermediate level of change. Thus, at this level there is a "first-order" effect on scattering due to valence type but no first-order effect due to the chemical identity of an ion within a valence type.

Figure 2b shows the raw viscosity data for the same experiments as Figure 1a. As expected, the shielding of the polyelectrolyte coils with increasing ionic strength leads to a decrease in solution viscosity. Interestingly, the maximum difference between the valence types occurs around 1 mM and then "closes up" to yield only a small difference in viscosity at high ionic strength. Again, the valence types create bands where the monovalent salts show the least change and the divalents show the most with respect to changes in I.

Figure 3a shows the square root of the slope d[$Kc/R(q,c)$]/dq^2 multiplied by the square root of $3M_w$ vs I. In the limit where interparticle interactions become q-independent (e.g., in eqs 15 and 16), this quantity becomes equal to R_g, which is defined as a convenient shorthand for the root-mean-square radius of gyration $\langle S^2\rangle^{1/2}$. R_g was obtained using the slope d[$Kc/R(q,c)$]/dq^2 in conjunction with eq 15 in the low q limit, and the R_g shown is computed for a mass of $M_w = 1.8 \times 10^6$. This is the average M_w obtained by extrapolating $Kc/R(q,c)$ to $q = 0$ and $c = 0$ at high values of I; all the added electrolytes yielded M_w values in this limit very close to this average. It is seen that, similar to the raw scattering and viscosity data, the R_g values for the different electrolyte ion classes cluster together in bands, which are separated distinctly from each other.

In Figure 3a the slope of Kc/R vs q^2 initially increases vs I. This is due to very strong intermolecular interactions at low I, which finally become sufficiently shielded that the slope yields R_g, which is, all the while, decreasing due to increasing I. This effect has been long recognized and studied.[49−51] In previous work it was possible to model the polymer as an electrostatically enhanced effective sphere and successfully fit the low I regime where intermolecular repulsion dominates the slope.[42] An angular maximum in scattering has also been observed for polyelectrolyte solutions at extremely low ionic strength.[52−54]

The inset to Figure 3a shows representative plots of $Kc/R(q,c)$ vs q^2 for 0.1 mg/mL HA in varying concentrations of $MgSO_4$. It is seen that, to a good approximation, these data are fit well with lines, and any predicted effects of excluded volume producing curvature[55−58] are not experimentally measurable. As mentioned, in this work a consistent use of eq 15 has been used, but previous work used eq 16.[36] Although deviations from linearity are not significant here, earlier work on narrow molecular mass fractions of high molecular weight polyelectrolytes were able to observe predicted deviations.[59]

Figure 3b shows $\langle S^2\rangle = 3M_w$d[$Kc/R$]/d$q^2$ from Figure 3a vs 1/sqrt[I (mM)], only over the regime where interparticle effects are no longer q-dependent (above about $I = 2$ mM). This representation is chosen because it gives a nearly linear trend at low values of 1/sqrt(I) as found in other works,[22,60−62] including Monte Carlo calculations.[63] Representative data for a monovalent salt, NaCl, and for an asymmetric divalent, $CaCl_2$ are shown. The solid lines in the curve are those due to calculations using combined electrostatic persistence length (EPL) and electrostatic excluded-volume (EEV) theories, *with no adjustable parameters*. This approach has been previously used with success in interpreting the effects of ionic strength and charge density on polyelectrolyte behavior. The computation requires the following experimentally or chemically known parameters: the apparent persistence length at extremely high ionic strength (175 Å for HA in monovalent salt, 131 Å in asymmetric divalent salt), the mass of the polymer (1.8×10^6), the contour length per monomer (10 Å), the mass per monomer (400 g mol^{-1}), the dielectric constant of the medium (78.3), the chain diameter (10 Å), and the number of elementary charges per Bjerrum length (0.7). (Using eq 16 brings $L_{p,0}'$ closer to the value of around 100 Å found earlier.[36])

Interestingly, the computed EEV/EPL curve with the expected value of $\xi = 0.7$ for HA falls virtually on top

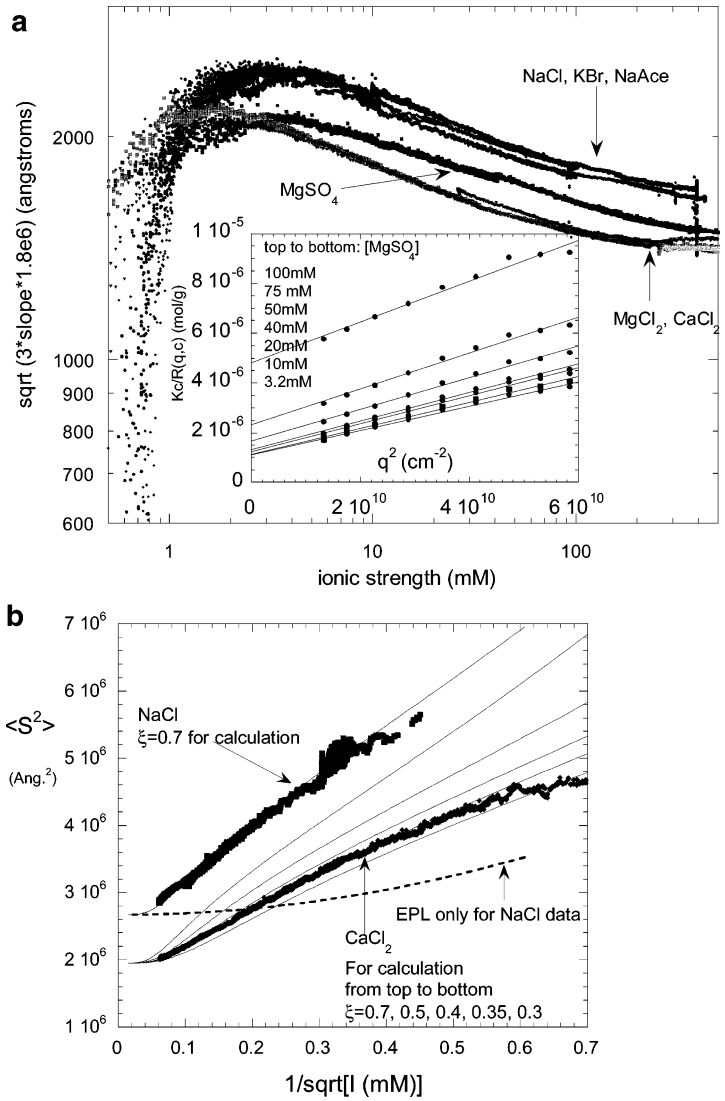

Figure 3. (a) The value for different salts of $[3M_w\text{slope}]$, where slope $= \mathrm{d}[Kc/R(q,c)/dq^2]$ and $M_w = 1.8 \times 10^6$. Above about 2 mM this quantity equals $R_g = \langle S^2\rangle^{1/2}$ and is given in angstroms. The inset shows the essentially linear nature of $Kc/R(q,c)$ vs q^2. (b) $\langle S^2\rangle$ from (a) for NaCl and $CaCl_2$. The solid lines show combined EPL/EEV calculations, with no adjustable parameters, as described in the text. The dashed line for the NaCl computation shows the effect of only considering EPL. The solid lines for the $CaCl_2$ calculation are for different values of the linear charge density ξ.

of the experimental data, whereas the same computation for the asymmetric divalents severely overestimates $\langle S^2\rangle$. The only parameter that can reasonably be affected, since the chemical structure of HA does not change, is ξ, for which calculations are shown based on the following values: $\xi = 0.7$, 0.5, 0.4, 0.35, 0.3. The curve for $\xi = 0.35$ falls very close to the experimental data, suggesting that the effective linear charge density of HA is lower with added divalent electrolyte. While counterion condensation of the "Manning type"[64] is expected for polyelectrolytes for which $\xi > 1$, and while the Bjerrum length shortens as $1/z^2$ for polyelectrolytes with ionic sites of charge z, there is no obvious reason that ξ for asymmetric divalents should be one-half its stoichiometric value. Further evidence of a lower charge density is presented below.

Before proceeding to the analysis of the other characteristics, it is pointed out that EEV provides the major part of the ionic strength dependent values of $\langle S^2\rangle$. To illustrate this, the dashed line in Figure 3b shows the prediction for HA in monovalent salt (i.e., for $\xi = 0.7$) using only the EPL notion. Similar results were found in earlier work[65] for HA in terms of the magnitude of the EEV, the values of $\langle S^2\rangle$, and $[\eta]$. The treatment of the relationship between EPL and EEV in that work, however, led to considerably lower estimates of $L_{p,0}$.

Another feature of EPL/EEV is that it is possible to estimate the true intrinsic persistence length $L_{p,0}$ of a polyelectrolyte at high values of I, using the high I value of apparent intrinsic persistence length L_0' and the high I value of A_2. The method for computing this was presented in detail in ref 29. The results here are that L_0 for HA is around 160 Å for the monovalent salts and around 110 Å for the asymmetric divalent salts. It is not obvious why the added salt should effect $L_{p,0}$ and in fact would seem to contradict the very notion of "intrinsic" persistence length. This is left as a puzzling and interesting phenomenon at this point. It may be tempting to suggest an actual counterion binding to the polyelectrolyte to describe this,[66] although the nonlinearity of the PB equation itself might be at root, as discussed below.

Figure 4 shows $[\eta]$ vs I computed from the values of η_r as explained above. The results of Figures 3a and 4 can be combined to examine the relationship between $[\eta]$ and R_g. Analyzing all the different salts yields $\gamma =$

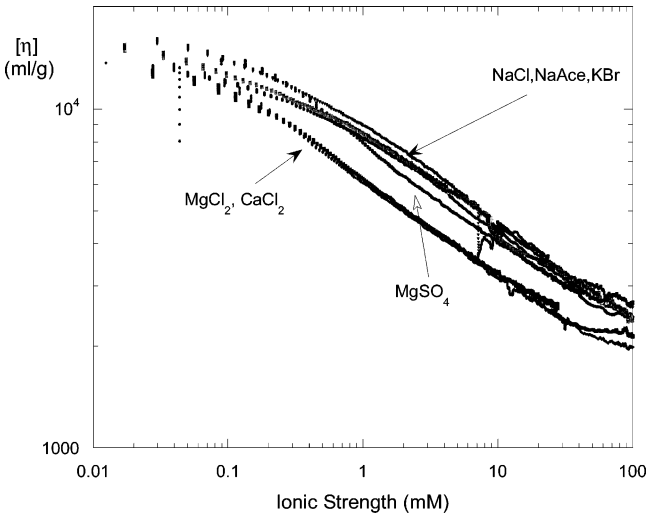

Figure 4. $[\eta]$ vs I for 0.1 mg/mL HA for different salts.

2.51 ± 0.34 in the relationship

$$[\eta] = AR_g^{\gamma} \tag{20}$$

This range is within reasonable expectation of the various viscosity theories mentioned, including the semiempirical Yamaka−Kurata[67] result of 2.43.

For a coil polymer at the Θ-point, the intrinsic viscosity is given by the Flory−Fox relation[68]

$$[\eta] = \frac{\Phi_v}{M}(\sqrt{6}\langle S^2\rangle^{1/2})^3 \tag{21}$$

where $\Phi_v = 2.56 \times 10^{23}$. Computing $\langle S^2\rangle^{1/2}$ via this relation, and terming it R_F (the Flory radius of gyration), it is found that for monovalents the average of the ratio R_F/R_g is 0.53, whereas for asymmetric divalents it is 0.61. This suggests that due to the higher level of contraction of the coil in divalent salts, there is less of a draining effect, and hence the R_F is closer to the ideal nondraining R_g. A separate work might examine the relationship between the κ_H, I, and the scaling behavior between $[\eta]$ and R_g.

Figure 5a shows A_2 vs I for the various salts. A_2 was computed by an iterative approach recently introduced.[42] There is no unique scaling law of A_2 vs I. EPL/EEV computations of A_2 (not shown) with no adjustable parameters yield only a qualitative match to the data and overestimate A_2 at high I and underestimate it at low I.

The fact that the divalents reach lower values of A_2 is consistent with the raw data of Figure 2a, in which the scattering of the divalents is stronger at higher salt than that of the monovalents. The values of A_2 change much more dramatically than those of R_g and $[\eta]$. This suggests that there may be a component to A_2 due purely to the electrostatic field, which is not reflected in the "hard" mass distributions that control R_g and $[\eta]$. Accordingly, Figure 5b shows a plot of A_2/R_g^3 as well as $A_2/[\eta]$ and $R_g^3/[\eta]$. (The dimensional units of these ratios are shown in the graph. We are not concerned with dimensionless units here, since the mass M of the polyelectrolyte is the same under all conditions and does not affect the trends of any of the ratios.) If A_2 were based on the purely steric interactions occasioned by the increase of R_g with decreasing I, then this value should be constant, as is essentially true for $R_g^3/[\eta]$ (qualified

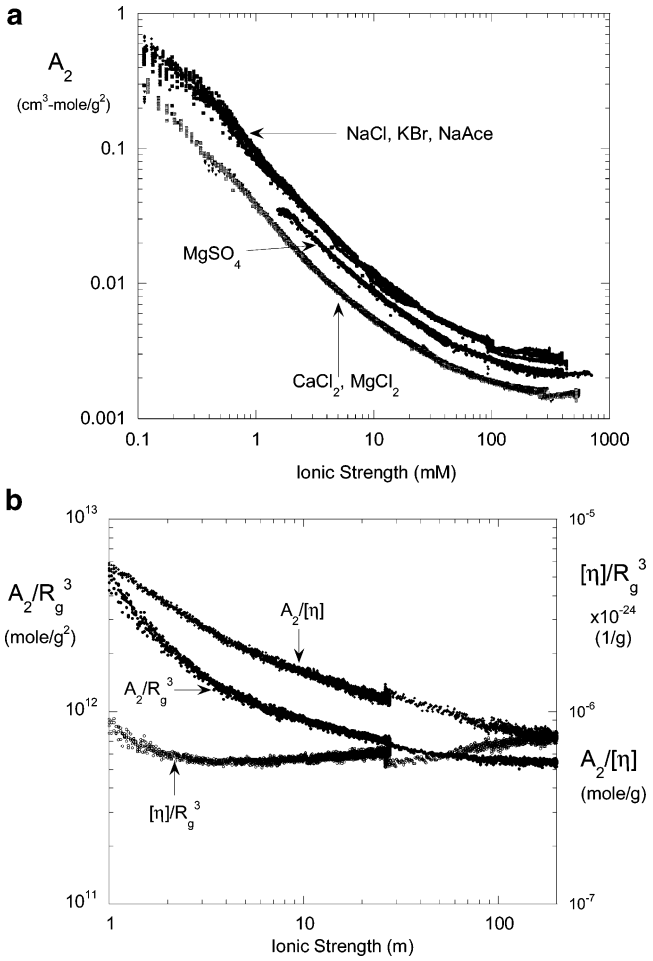

Figure 5. (a) A_2 vs I for the different salts. (b) Comparative quantities A_2/R_g^3, $[\eta]/R_g^3$, and $A_2/[\eta]$, suggesting that A_2 has a nonsteric, purely electrostatic portion that increases as I decreases.

by the above comments on the empirical scaling law between R_g and $[\eta]$). It is seen, however, that both A_2/R_g^3 and $A_2/[\eta]$ increase as I decreases. This suggests that the intermolecular interaction can be decomposed into two components: The sterically based component measured by an electrostatically sensitive R_g (and measured also largely by $[\eta]$) and a component due purely to the interaction of the electrostatic fields of each polyelectrolyte in an encounter. It can be surmised that this field would increase the excluded volume beyond that of caused by R_g alone, as seen to be true in Figure 5b, and also that this field interaction would have no direct effect on the intrinsic polyelectrolyte friction of each chain and hence would not affect the friction directly.

This suggests an analysis in terms of an equivalent, extensible, charged sphere model; that is, eq 4 can be decomposed into

$$A_2 = A_{2,R_g} + A_{2,\text{electrostatic}} \tag{22}$$

where $A_{2,\text{electrostatic}}$ goes to zero at high values of I and its potential $U_{el}(r_{12})$ is operative for $r_{12} > 2R_g$. A_{2,R_g} can be simplified to an equivalent hard sphere, whose contribution to A_2 is given by the first right-hand term in eq 4, and $R_{eq} = aR_g$, where a is the proportionality constant between the measured R_g and the radius of the equivalent sphere R_{eq}. a can be found by extrapolating A_2/R_g^3 to infinite I. This was done by plotting the

latter quantity vs 1/sqrt(I) and extrapolating to the origin. The average value of a is 0.55 for all salts.

$A_{2,\text{electrostatic}}$ is computed from the experimental values of A_2 and R_g according to

$$A_{2,\text{electrostatic}} = A_2 - \frac{16\pi N_A (aR_g)^3}{3M^2} \qquad (23)$$

where $a = 0.55$ and $M = 1.8 \times 10^6$. Figure 6a shows the result for all the salts. Remarkably, $A_{2,\text{electrostatic}}$ follows a fairly well-defined scaling law of the form

$$A_{2,\text{electrostatic}} = BI^{\sigma} \qquad (24)$$

where $\sigma = 1.07 \pm 0.07$ and whose prefactor B is quite different and clustered according to electrolyte valence and symmetry: $B = 0.076$ for monovalents, $B = 0.058$ for the single symmetric divalent, and $B = 0.028$ for the two asymmetric divalents. Just as the EPL/EEV predicted behavior of $\langle S^2 \rangle$ vs I suggests that the linear charge density ξ is different for divalents, these prefactor differences are a clue that the magnitude of the potential in and around the polyelectrolyte chains decreases with increasing valence.

An illustration of where the R_g and electrostatic portions of A_2 dominate is given in Figure 6b for a monovalent (NaCl) and asymmetric divalent ($MgCl_2$). In both cases A_{2,R_g} dominates above about $I = 10$ mM, at which ionic strength there is a crossover, and below it, $A_{2,\text{electrostatic}}$ dominates by an order of magnitude by the time 1 mM is reached. A_{2,R_g} has been truncated at about $I = 2$ mM, since R_g can no longer be measured below that value, and $A_{2,\text{electrostatic}}$ becomes approximately equal to A_2. The fact that the A_{2,R_g} defined by R_g (i.e., proportional to ${R_g}^3 = \langle S^2 \rangle^{3/2}$) scales as $\kappa^{-3/2}$ highlights the qualitatively different nature of this steric contribution to A_2 when contrasted to the κ^{-2} contribution of the purely electrostatic field portion $A_{2,\text{electrostatic}}$.

To analyze the contribution due purely to the electrostatic field, $A_{2,\text{electrostatic}}$, the result of Verway and Overbeek can be invoked for the potential between two spheres of radius R, when $\kappa R \gg 1$, which is the case here, since $R > 10^3$ Å and $1/\kappa < 100$ Å for the regime $I = 1$ mM to 1 M.

$$U(r_{12}) \cong 2\pi\epsilon R\phi(R)^2 \ln[1 + \exp(-2\kappa R x)] \qquad (25)$$

where

$$x = (r_{12} - 2R)/2R \qquad (26)$$

where r_{12} is the interparticle center-to-center distance. A subtlety arises in the computations. Namely, if $2R_{eq}$ is used for the beginning of the $A_{2,\text{electrostatic}}$ integration, where $R_{eq} = aR_g$, then the computed $A_{2,\text{electrostatic}}$ seriously underestimates the experimental values. A simple hard sphere with external electrostatic atmosphere is hence inadequate. Instead, consider that the polyelectrolyte coil has actually only a semihard, or even soft, potential, since interpenetration of coils is possible. Hence, $2R_g$, as computed by the EPL/EEV model was used for $2R$, the beginning of the $A_{2,el}$ integration.

Following this notion of a polymer with radius R_g and a field beyond R_g causing the interaction $U(r_{12})$ given by eq 25 and substituting into eq 4 yields interesting results. Namely, the model gives a fairly good fit to the data, especially at higher values of I. Figure 6c shows calculations of $A_{2,\text{electrostatic}}$ for a typical monovalent salt (NaCl) and an asymmetric divalent ($CaCl_2$). The one adjustable parameter was the surface potential at zero screening. The inset shows the surface potential of the equivalent sphere, which is the unscreened surface potential reduced by the factor $1/(1 + \kappa R)$, as per eq 3. At lower I the surface potential becomes larger than kT, so it is expected that the approximate expression above will become progressively inaccurate. Nonetheless, the notion of the pure electrostatic potential captures a number of important features of the data. At moderate to high ionic strength it predicts $A_{2,\text{electrostatic}}$ quite well and gives the same type of "pseudo-scaling" law. Importantly, the surface potential of the equivalent sphere is significantly lower for the asymmetric divalent salt than for the monovalent salt. This is consistent with the EPL/EEV results above. It is also gratifying to see that the result of the EPL/EEV for R_g provides robust values in eqs 4 and 25, to which $A_{2,\text{electrostatic}}$ is fairly sensitive.

The thickness of the electrostatic atmosphere can be defined as the region from R_g to the value of x where $1 - e^{-U(x)/kt} = 0.5$. The thickness determined this way runs from as high as 420 Å for the monovalent case at $I = 1$ mM to 23 Å for the monovalent case at $I = 100$ mM.

To gauge the magnitude of the R_g contribution to A_2, it is assumed that a finite square well potential exists, with a mean value $\langle U \rangle$ for $0 < r_{12} < 2R_g$. This can be found from

$$e^{-\langle U \rangle/kT} = 1 - \frac{3M^2 A_{2,R_g}}{16\pi N_A {R_g}^3} \qquad (27)$$

and yields about $\langle U \rangle = 0.19kT$. Hence, the potential is fairly "soft". This model of a soft core, expansible sphere with an electrostatic atmosphere is in contrast to fixed sphere models that have successfully been used to model structures such as micelles.[69−71] Interestingly, Welch and Hoagland recently found that charged dendritic polyelectrolytes could be exceptionally well modeled by a charged, ion impenetrable sphere.[72]

As to the mechanism whereby potentials increase in the order asymmetric divalent < symmetric divalent < symmetric monovalent, one conjecture follows immediately from consideration of the nonlinear PB equation

$$\nabla^2\phi = \frac{-c_s}{\epsilon}\{az_a \exp[-z_a e\phi/kT] - bz_b \exp[z_b e\phi/kT]\} \qquad (28)$$

where the electrolyte is of the form A_aB_b, z_a and z_b are the absolute values of the number of elementary charges on each ion, where $az_a = bz_b$ for electroneutrality of the undissociated electrolyte, c_s is the added (bulk) electrolyte concentration, and ϵ is the solvent dielectric constant, taken to be that of water. c_s times the bracketed expression is the net charge density around the polyelectrolyte due to the unequal distribution of the electrolyte ions. For the monovalent case, $a = b = z_a = z_b = 1$, for the symmetric divalent case $a = b = 1$, $z_a = z_b = 2$, and for the asymmetric divalent case $a = 1$, $b = 2$, $z_a = 2$, $z_b = 1$. Using the relationship between ionic strength I and c_s the charge density $\rho(\phi(r))$ can be

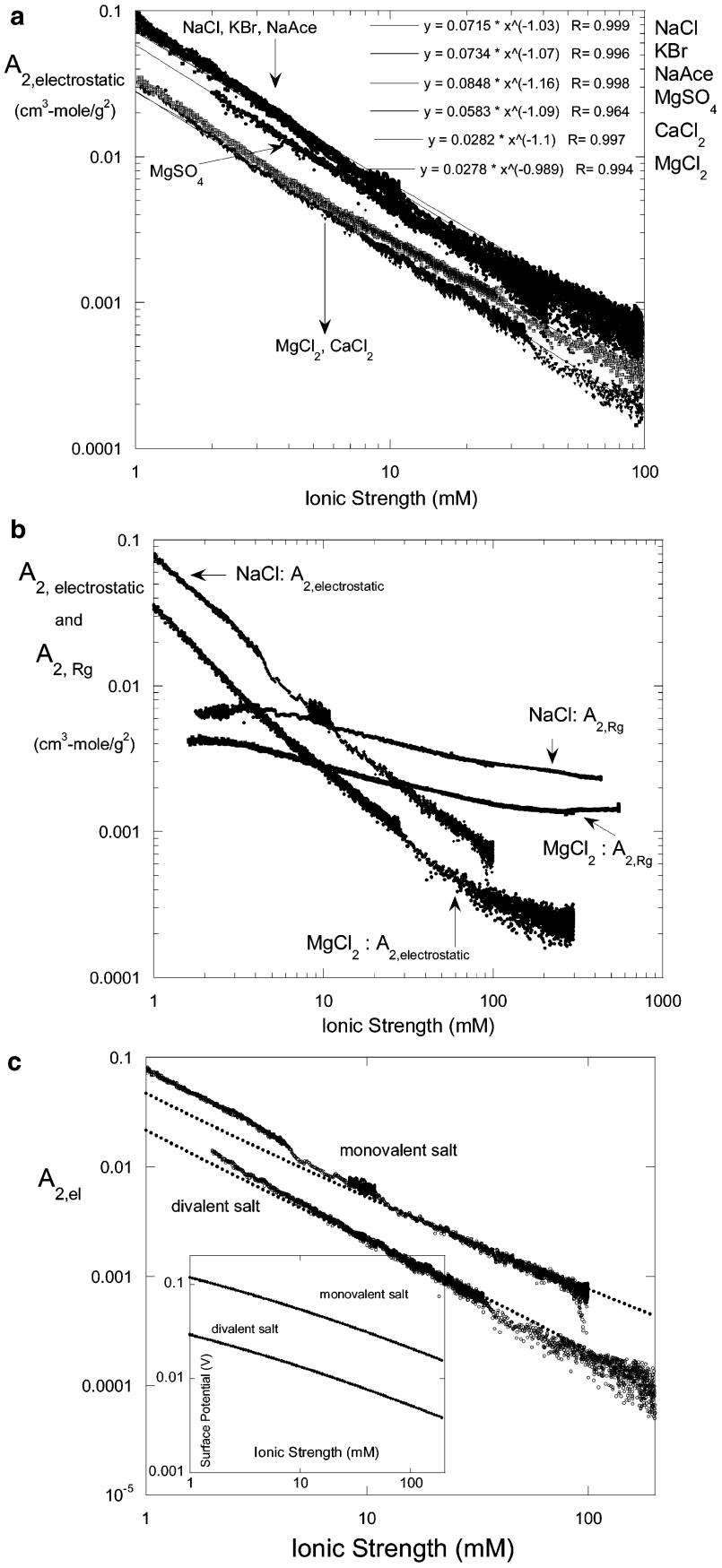

Figure 6. (a) The electrostatic component of A_2, termed $A_{2,\text{electrostatic}}$, showing a scaling law of $I^{-1.07}$, with prefactors that are smaller for divalent salts. (b) A comparison of the R_g ("soft core") and electrostatic A_2 contributions, A_{2,R_g} and $A_{2,\text{electrostatic}}$, which clearly shows the crossover to purely electrostatic domination at I below about 10 mM. (c) Computation of $A_{2,\text{electrostatic}}$, using the soft-core, expansible equivalent charged sphere model. The inset shows the single adjustable parameter, the surface potential (at R_g) of the equivalent sphere for the monovalent and asymmetric divalent cases.

written for each case as

$$\rho(\phi) = I\{\exp[-e\phi/kT] - \exp[e\phi/kT]\},$$
monovalent case (29a)

$$\rho(\phi) = \frac{I}{2}\{\exp[-2e\phi/kT] - \exp[2e\phi/kT]\},$$
symmetric divalent case (29b)

$$\rho(\phi) = \frac{2I}{3}\{\exp[-2e\phi/kT] - \exp[e\phi/kT]\},$$
asymmetric divalent case (29c)

When these are plotted using negative potentials, since HA is a negatively charged polyelectrolyte, $\rho(\phi)$, which is positive, at any given value of ϕ, grows most quickly for eq 29c, followed by eq 29b and then eq 29a. Only for the case $ze\phi/kT \ll 1$, i.e., for the linearized PB equation, do expressions 29a−c converge to the same dependence on ϕ. In the full nonlinear form, however, the divalent cations cluster more closely to the polyelectrolyte's anionic charge distribution and for the asymmetric divalent case the singly charged anions drop off more slowly than the divalent cations, giving the greatest charge density around the polyanionic charge. This effect should be reflected in correspondingly lower potentials for asymmetric divalents when the nonlinear PB is solved. This is not undertaken here. The point is taken, however, that the linearized PB equation groups the valence and symmetry of the electrolyte into the single constant I and leads to predictions that potentials and charge distributions should be only a function of I. The above argument, however, shows that charge distributions, and ultimately potentials, are not merely a function of I, and the trends seen throughout this work can be consistently rationalized from this point of view.

Second-Order Effects: Ion Species. As seen above, the results from each valence and symmetry class of added electrolyte cluster rather closely together, making differences in these properties the origin of the first-order effects. Measurable second-order effects do occur, however, when the ion species in a valence and symmetry class changes.

It was found that a good way of monitoring these small differences in behavior with ACM is to ramp continuously from one salt type to another at fixed ionic strength and polyelectrolyte concentrations. As a first illustration, a ramp between valence classes producing first-order effects is given. Figure 7a shows an example of the procedure, where 0.1 mg/mL HA was ramped between 10 mM ionic strength solutions of NaCl, $CaCl_2$, and $MgSO_4$. The excess scattering (total scattering at 90° minus 0.16 V baseline) in going from NaCl to $CaCl_2$ increases by 60%, and in $MgSO_4$ the scattering is 15% higher than in NaCl, consistent with Figure 2a, which was performed separately. The viscosity drops 28% from NaCl to $CaCl_2$ and 12% from NaCl to $MgSO_4$. It is also significant to point out how well the data are reproduced in two completely different types of experiments; the salt ramp at fixed [HA] in Figure 2a and a ramp between reservoirs of different salts at the same value of I and [HA]. Figure 7b shows $\langle S^2 \rangle$ and A_2 data for the Figure 7a data.

This ramping technique is well adapted to measuring smaller changes in behavior, since the detectors are working under identical conditions. Figure 8a shows ramps at 100 mM ionic strength and 0.1 mg/mL HA between monovalent salts with the same cation: NaI, NaCl, and NaF. It is found that intensity increases (baseline 0.16 V) in the order I < Cl < F by 12% and 19% for Cl and F compared to I, respectively. Oddly, the viscosity also increases (baseline 3.39 V) in the same order by 8% and 20%, unlike all other cases where an increase in light scattering was accompanied by a decrease in viscosity. The magnitude of these effects is pronounced but significantly smaller than for change of valence class. Hence, changing anion type within a valence class (here, monovalents) can be considered to produce second-order effects in scattering and viscosity. Figure 8b shows the corresponding R_g and A_2 data for Figure 8a. The change in A_2 from NaF to NaI is about 42% compared to over 100% changing from monovalent to asymmetric divalent.

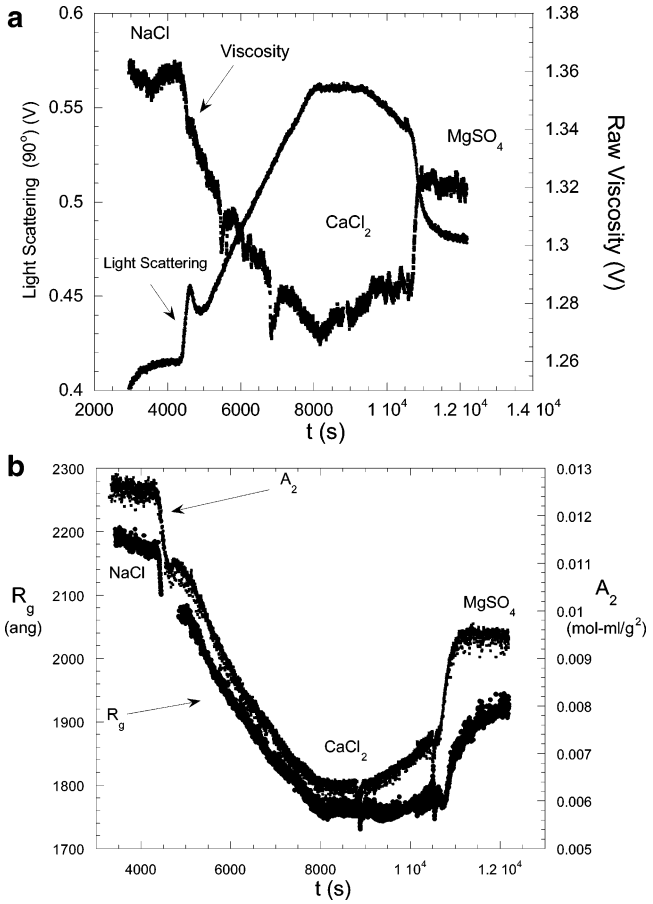

Figure 7. (a) Use of ACM to probe constant polymer concentration (0.1 mg/mL HA) and ionic strength (I = 10 mM). Light scattering (90°) baseline was 0.16 V, and viscosity baseline was 1.02 V. (b) The R_g and A_2 results from (a). These can be cross-checked with Figures 3a and 5a, respectively.

Figure 9a shows the effect of changing the cation for monovalent salts, while keeping the same anion: NaCl, CsCl, and KCl. In this case, light scattering and viscosity proceed in opposite directions, as usual. For light scattering Cs > K ∼ Na, and for viscosity Na > K > Cs. The maximum change in both viscosity and light scattering is a mere 7% (Cs vs Na), a weak "second-order" effect. For Figure 9a, for monovalent salts with different counterions, the effects are small. Again, it is seen that an increase in light scattering goes in the same direction as the increase in the size of the ion, which agrees with ref 13. Figure 9b shows the values of A_2 and R_g for Figure 9a.

The effects of different co-ions in the case of monovalent salts is seen to have a larger effect than that of the

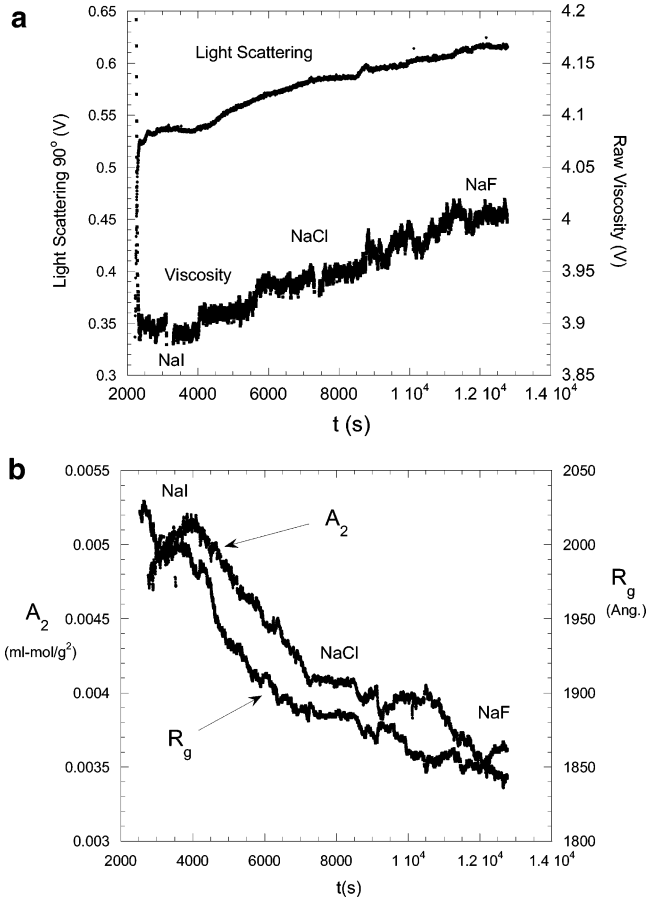

Figure 8. (a) Variation of the electrolyte anion at constant ionic strength, 100 mM, and constant concentration of HA of 0.1 mg/mL. Light scattering baseline (90°) was 0.16 V, and viscosity baseline was 3.39 V. (b) The R_g and A_2 results from (a).

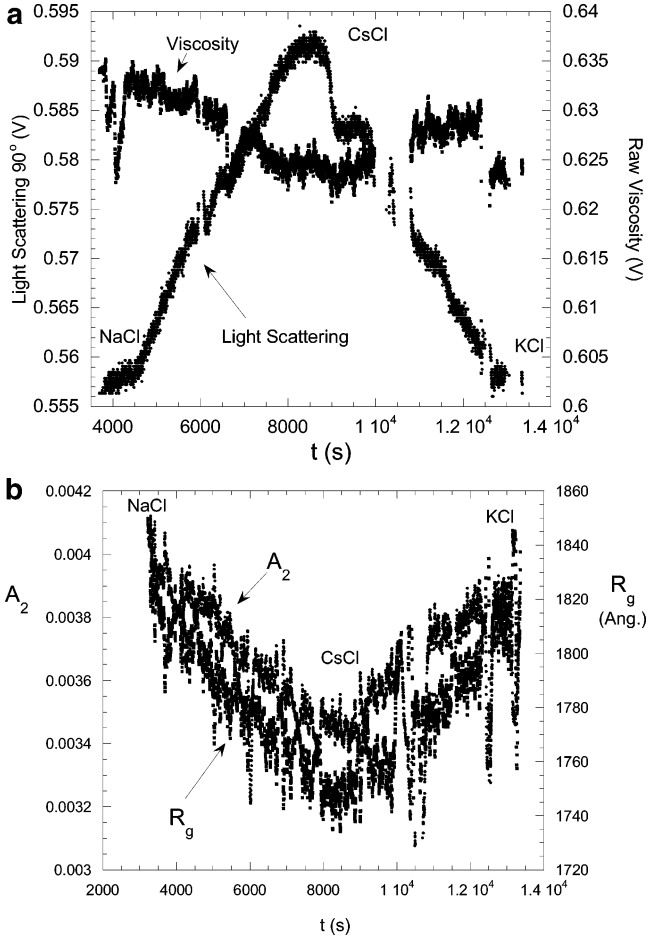

Figure 9. (a) Effect of varying the electrolyte cation for 0.1 mg/mL HA at constant ionic strength, 10 mM. Light scattering (90°) baseline was 0.10 V and 0.496 for viscometer. (b) The R_g and A_2 results from (a).

counterions. The effects follow the solvation energies for these ions,[73−75] but remarkably, in contrast to the other cases, both light scattering intensity and viscosity fall as the series F−Cl−I is traversed. This follows the order of decreasing solvation energy, so it might be conjectured that the less solvated I entrains less water into the overall vicinity of the polyion, leading to decreased hydrodynamic volume and hence decreased viscosity. At the same time, the bulky I ions in the vicinity may lead to a small, sterically based increase in the *static* dimensions of the polyanion and hence to an increase in A_2 and a decrease in scattering. While this conjecture may appear counterintuitive, the overall notion is that hydrodynamic volume can decrease because of decreased solvated volume, at the same time that coil expansion occurs due to steric effects.

All experiments show that the conformational/interaction changes are smooth. The question arises as to what conditions are required to induce a "phase transition" in conformation and/or interaction of HA. For example, addition of NaOH caused a titration-curve-dependent destiffening of HA,[76] whereas use of "oligocations" (e.g., histones) and polycations (e.g., PLL) can lead to microgel formation, so the question arises what valence, charge density, or other conditions are required of the positive oligoions to cause this.

Conclusions

There are first-order differences in polyelectrolyte conformations, interactions, and hydrodynamics when electrolytes of different valence and symmetry are added to the polyelectrolyte solution. Each relevant characteristic, however, bears the same scaling relationship to ionic strength I, but the prefactors are different. EPL/EEV calculations without adjustable parameters suggest that the effective linear charge density is considerably lower in the presence of divalent ions than monovalent ions. Furthermore, the electrostatic portion of A_2, termed $A_{2,\text{electrostatic}}$, shows lowered electrostatic potentials in the vicinity of the polyelectrolyte when divalent ions are present compared to when monovalent ions are present. Consideration of the nonlinear PB equation shows that charge distributions, and ultimately potential, are not merely a function of I but depend on the details of the electrolyte valence and symmetry. The asymmetric divalents give a tighter shielding of the polyanion charge, leading to lower potentials.

The entire behavior of $\langle S^2 \rangle$ and A_2 is summarized by an equivalent, soft-core, expansible, charged-sphere model. The data and these notions supply grist for a more detailed quantitative model that would use the nonlinear PB for an expansible, ion-permeable sphere, whose dimensions would make self-consistent use of the EPL/EEV theory.

Second-order effects in these properties are seen when the chemical identity of the anion is changed for a given symmetry and valence class, and yet weaker second-order effects are seen when changing the cation in a

given class. These effects are rationalized in terms of a Hoffmeister series.[77,78]

Hence, to first order, for polyelectrolytes that do not undergo phase transitions, polyelectrolyte theories that treat added electrolyte as point charges are good approximations, although second-order effects appear due purely to the chemical identity of the electrolyte ions. In cases where phase transitions occur, rather than the monotonic behavior shown by HA, the chemical identity of the ions can become more important than symmetry and valence considerations alone.

The ACM technique should prove a valuable means of quantitatively assessing ion type effects for a wide range of polyelectrolytes, especially those which show ion specific condensation and collapse phenomena.

Acknowledgment. Support from NSF CTS-0124006, NASA NAG-1-02070, and NCC3-946 is gratefully acknowledged as well as summer support for G. A. Sorci from the Hearin foundation, received through the Millsaps College faculty development committee.

References and Notes

(1) Forster, S.; Schmidt, M. *Adv. Polym. Sci.* **1995**, *120*, 53.
(2) Ninham, B. W.; Yaminsky, V. *Langmuir* **1997**, *13*, 2097.
(3) Comper, W. D.; Laurent, T. C. *Physiol. Rev.* **1978**, *58*, 322.
(4) Benegas, J. C.; Cesaro, A.; Rizzo, R.; Paoletti, S. *Biopolymers* **1998**, *45*, 203.
(5) Tomac, S.; Sakar, M.; Ratliainen, T.; Wittung, P.; Nielsen, P. E.; Norden, B.; Graslund, A. *J. Am. Chem. Soc.* **1996**, *118*, 5544.
(6) Viebke, C.; Piculell, L.; Nilsson, S. *Macromolecules* **1994**, *27*, 4160.
(7) Nilsson, S.; Piculell, L.; Jonsson, B. *Macromolecules* **1989**, *22*, 2367.
(8) Flory, P. J.; Osterheld, J. E. *J. Phys. Chem.* **1959**, *58*, 653.
(9) Verwey, E. J. W.; Overbeek, J. Th. G. In *The Theory of the Stability of Lyophobic Colloids*; Elsevier: New York, 1948.
(10) Kruyt, H. R.; van der Made, H. *Rec. Trav. Chim.* **1923**, *42*, 277.
(11) Orofino, T. A.; Flory, P. J. *J. Chem. Phys.* **1959**, 283.
(12) Vrij, A.; Overbeek, J. Th. G. *J. Colloid Sci.* **1962**, *17*, 570.
(13) Beer, M.; Schmidt, M.; Muthukumar, M. *Macromolecules* **1997**, *30*, 8375.
(14) Oesterberg, R.; Persson, D.; Bjursell, G. *J. Biomol. Struct. Dyn.* **1984**, *2*, 285.
(15) Bloomfield, V. A.; Wilson, R. W.; Rau, D. C. *Biophys. Chem.* **1980**, *11*, 339.
(16) Rau, D. C.; Parsegian, V. A. *Biophys. J.* **1992**, *61*, 260.
(17) Rau, D. C.; Parsegian, V. A. *Biophys. J.* **1992**, *61*, 246.
(18) Gelbart, W. M.; Bruinsma, R. F.; Pincus, P. A.; Parsegian, V. A. *Phys. Today* **2000**, 38.
(19) Chaires, J. B.; Norcum, M. T. *J. Biol. Struct. Dyn.* **1988**, *5*, 1187.
(20) A_3 was not determined in this work, as was done in ref 42. It requires repeating electrolyte ramps at higher polyelectrolyte concentration and then using the iterative methods of ref 42.
(21) Landau, L. D.; Lifschitz, E. M. In *Statistical Physics*, 3rd ed.; Pergamon Press: Oxford, 1963; Part 1, Chapter 12.
(22) Reed, W. F. In *Macroion Characterization*; Schmitz, K., Ed.; American Chemical Society: Washington, DC, 1994.
(23) Odijk, T. *J. Polym. Sci., Phys. Ed.* **1977**, *15*, 477.
(24) Odijk, T.; Houwaart, A. C. *J. Polym. Sci., Polym. Phys. Ed.* **1978**, *16*, 627.
(25) Skolnick, J.; Fixman, M. *Macromolecules* **1977**, *10*, 9444.
(26) Fixman, M.; Skolnick, J. *Macromolecules* **1978**, *11*, 863.
(27) Gupta, S. K.; Forsman, W. C. *Macromolecules* **1972**, *5*, 779.
(28) Reed, W. F.; Reed, C. E. *J. Chem. Phys.* **1991**, *93*, 8479.
(29) Reed, W. F.; Ghosh, S.; Medjahdi, G.; Francois, J. *Macromolecules* **1991**, *24*, 6189.
(30) Yamakawa, H.; Fujii, M. *Macromolecules* **1973**, *6*, 407.
(31) Davis, R. M.; Russell, W. B. *J. Polym. Sci.* **1986**, *24*, 511.
(32) Mulderje, J. J. H.; Jalink, H. L. *Macromolecules* **1987**, *20*, 1152.
(33) Muthukumar, M. *J. Chem. Phys.* **1987**, *86*, 7230.
(34) Muthukumar, M. *J. Chem. Phys.* **1996**, *105*, 5183.
(35) Berry, G. C. *Adv. Polym. Sci.* **1994**, *114*, 233.
(36) Ghosh, S.; Li, X.; Reed, C. E.; Reed, W. F. *Biopolymers* **1990**, *30*, 1101.
(37) Personal communication from Dr. Raymond Farinato, CYTEC Industries, Stamford, CT.
(38) Ogston, A. G.; Preston, B. N. *J. Biol. Chem.* **1966**, *1*, 241.
(39) Buhler, E.; Rinaudo, M. *Macromolecules* **2000**, *33*, 2098.
(40) Strelitzki, R.; Reed, W. F. *J. Appl. Polym. Sci.* **1999**, *73*, 2359.
(41) Bayly, E. E.; Brousseau, J. L.; Reed, W. F. *Int. J. Polym Anal. Charact.* **2002**, *7*, 1.
(42) Sorci, G. A.; Reed, W. F. *Macromolecules* **2002**, *35*, 5218.
(43) Sorci, G. A.; Reed, W. F. *Langmuir* **2002**, *18*, 353.
(44) Basu, S. *Nature (London)* **1951**, *168*, 341.
(45) Fuoss, R. M.; Strauss, V. P. *J. Polym. Sci.* **1948**, *3*, 602.
(46) Fouissac, E.; Milas, M.; Rinaudo, M.; Borsali, R. *Macromolecules* **1992**, *25*, 5613.
(47) Cohen, J.; Priel, Z.; Rabin, J. *J. Chem. Phys.* **1988**, *88*, 7111.
(48) Reed, W. F. *J. Chem. Phys.* **1994**, *101*, 2515.
(49) Hansen, J. P. In *Theory of Simple Liquids*; Academic Press: New York, 1986.
(50) Hayter, J. B.; Penfold, J. *Mol. Phys.* **1981**, *42*, 109.
(51) Benmouna, M.; Weill, G.; Benoit, H.; Akcasu, Z. *J. Phys.* (*Paris*) **1982**, *43*, 1679.
(52) Nierlich, M.; Williams, C. E.; Boue, F.; Cotton, J. P.; Daoud, M.; Farnoux, B.; Jannink, G.; Picot, C.; Moan, M.; Wolff, C.; Rinaudo, M.; de Gennes, P. G. *J. Phys.* (*Paris*) **1979**, *40*, 701.
(53) Drifford, M.; Dalbiez, J. P. *J. Phys. Chem.* **1984**, *88*, 5368.
(54) Li, X.; Reed, W. F. *J. Chem. Phys.* **1991**, *94*, 4568.
(55) Ohta, T.; Oono, Y..; Freed, K. *Phys. Rev. A* **1982**, *25*, 2801.
(56) Loucheux, C.; Weill, G.; Benoit, H. *J. Chim. Phys.* **1958**, *55*, 540.
(57) Sharp, P.; Bloomfield, V. A. *Biopolymers* **1968**, *6*, 1201.
(58) Reed, C. E.; Reed, W. F. *J. Chem. Phys.* **1992**, *97*, 7766.
(59) Kitano, T.; Taguchi, A.; Noda, I.; Nagasawa, M. *Macromolecules* **1980**, *13*, 57.
(60) Tricot, M. *Macromolecules* **1984**, *17*, 1698.
(61) Fisher, L. W.; Sochor, A. R.; Tan, J. S. *Macromolecules* **1977**, *10*, 955.
(62) Reed, W. F.; Ghosh, S.; Hedjahdi, G.; Francois, J. *Macromolecules* **1991**, *24*, 6189.
(63) Reed, C. E.; Reed, W. F. *J. Chem. Phys.* **1991**, *94*, 8479.
(64) Manning, G. S. *J. Chem. Phys.* **1969**, *51*, 924.
(65) Hayashi, K.; Tsutsumi, K.; Nakajima, F.; Norisuye, T.; Teramoto, A. *Macromolecules* **1995**, *28*, 3824.
(66) Strauss, U. P.; Woodside, D.; Wineman, P. *J. Phys. Chem.* **1957**, *61*, 1353.
(67) Kurata, M.; Yamakawa, H. *J. Chem. Phys.* **1958**, *29*, 311.
(68) Flory, P. J.; Fox, T. G. *J. Am. Chem. Soc.* **1951**, *73*, 1904.
(69) Dorshow, R.; Briggs, J.; Bunton, C. A.; Nicoli, D. F. *J. Phys. Chem.* **1982**, *86*, 2388.
(70) Corti, M.; Degiorio, V. *J. Phys. Chem.* **1981**, *85*, 711.
(71) Baptista, M. S.; Cuccovia, I.; Chaimovich, H.; Politi, M. J.; Reed, W. F. *J. Phys. Chem.* **1992**, *96*, 6442.
(72) Welch, C. F.; Hoagland, D. A. *Langmuir* **2003**, *19*, 1082.
(73) Berry, R. S.; Rice, S. A.; Ross, J. In *Physical Chemistry*, 2nd ed.; Oxford University Press: New York, 2000; Chapter 26.
(74) Collins, K. D. *Biophys. J.* **1997**, *72*, 65.
(75) Wright, E. M.; Diamond, J. M. *Physiol. Rev.* **1977**, *37*, 23.
(76) Ghosh, S.; Kobal, I.; Zanette, D.; Reed, W. F. *Macromolecules* **1993**, *26*, 4685.
(77) Hunter, R. J. *Foundations of Colloid Science*; Oxford University Press: New York, 1989; Chapter 6.
(78) Fixman, M. *J. Chem. Phys.* **1964**, *41*, 3772.

MA035551Z